HIAPER Cloud Radar (HCR) Preliminary Design

Eric Loew and Gordon Farquharson
Earth Observing Laboratory
National Center for Atmospheric Research

1. Background

The HIAPER cloud radar (HCR) initiative provides an opportunity for expanding the envelope of airborne radar systems by delivering high spatial and temporal resolution observations with improved accuracy in comparison to existing airborne millimeter wavelength radars. Requirements for cloud and precipitation radar remote sensing are very stringent due to the need for high sensitivity (> -25 dBZ @ 10 km) and wide dynamic range of received signal strengths (90 dB or more). The intent of this document is to outline the preliminary design of an airborne millimeter wave radar to satisfy the observational needs of the atmospheric research community.

Desired HCR features were distilled from responses to a selectively distributed scientific community survey, a thorough examination of millimeter wave radar technologies, and input provided in discussions with engineers and scientists at JPL, NASA Goddard, and the University of Wyoming. These discussions led to a proposed millimeter wave radar system which is capable of measuring both spectral moments and the polarimetric scattering matrix with sufficient sensitivity and accuracy to be useful in the study of cloud microphysics. Given cost constraints, and to obtain the greatest spatial coverage, the vast majority of the radar system will be housed in HIAPER's 20" wing pod, designated the NCAR pod. EOL staff considered four designs incorporating a pod-based polarimetric scanning radar (dual-wavelength: K_a- and W-band, matched or unmatched beams, and dual-Doppler: K_a- or W-band). Based on the results of community surveys, EOL recommended building a polarimetric Doppler dual-wavelength (K_a- and W-band) radar with both matched and unmatched beam configurations in a pod. The cost of this dual wavelength system eclipsed the available MREFC funds, and a phased development approach was adopted. The phase A system will consist of a pod mounted W-band Doppler radar. In phase B, pulse compression and polarimetric capabilities will be added. In phase C, the K_a-band radar will be added. At this point, only phase A is funded and it is this system design that this document supports; however, the phase A system will be designed so as to incorporate the electronic and mechanical requirements of phases B and C.

2. System Requirements

This section establishes the requirements for the HCR over a broad range of criteria. These include radar performance, a reasonable upgrade path, system size and weight constraints, operating environment, external power and signal needs, radar calibration, and remote and/or autonomous operation. These requirements will form the basis for a preliminary system design.

2.1. Performance

The system performance is evaluated on spatial coverage and temporal resolution, radar sensitivity, range/velocity ambiguity, and velocity and reflectivity accuracy. Sections 2.1.1 to 2.1.4 present the specifications for each of these criteria.

2.1.1. Spatial Coverage

During the HCR feasibility study, it was determined that the radar should be capable of

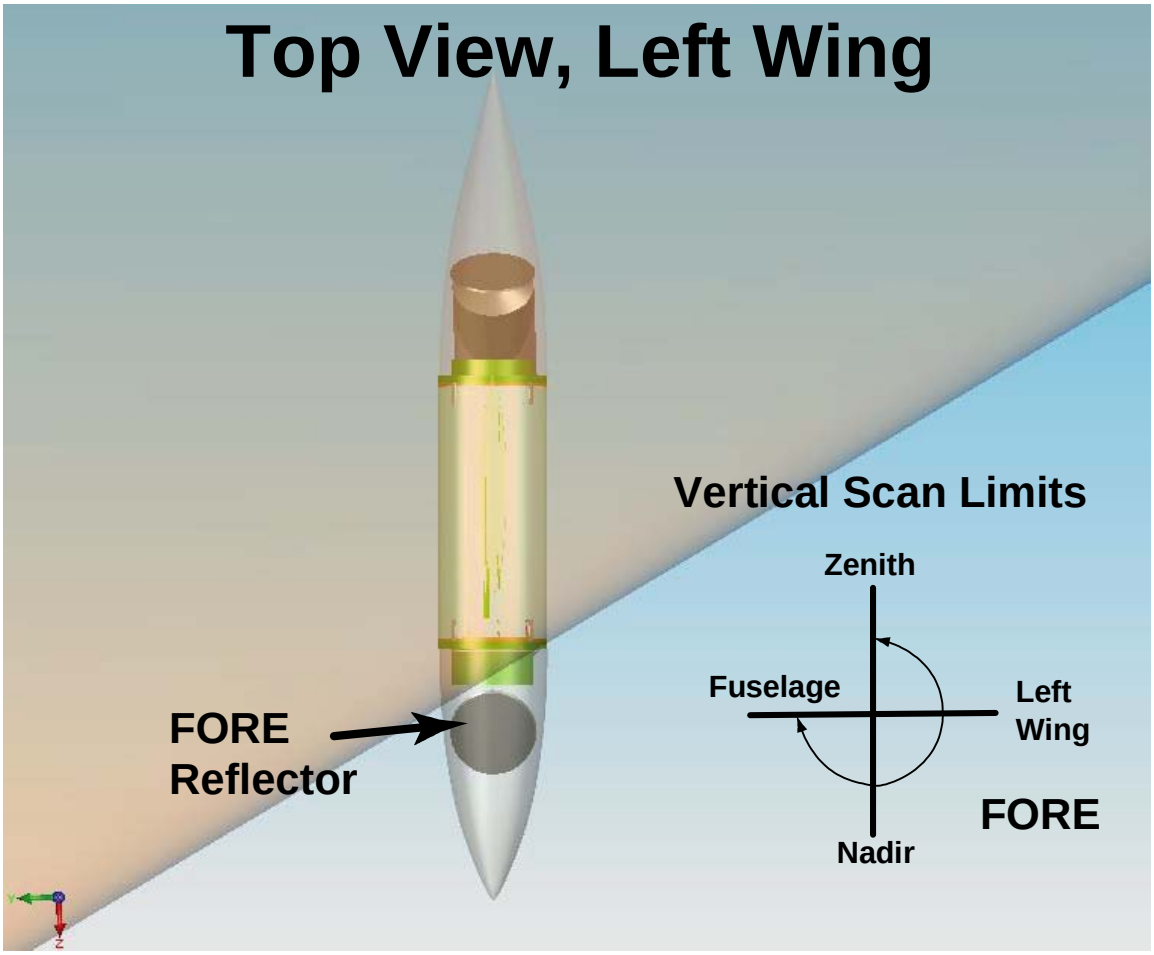

Figure 1: The radar will be able to scan from zenith to through nadir, and towards to the fuselage of the aircraft.

steering the beam at least 180 degrees from zenith to nadir in the vertical plane normal to the vertical plane of the longitudinal axis of the aircraft (Figure 1). It is also highly desirable to keep the radar beam within the vertical cross-track plane to avoid introducing a significant component of aircraft velocity into the measured velocity.

2.1.2. Sensitivity

Sensitivity or minimum detectable signal (MDS) requirements for millimeter wave radars are almost exclusively specified post incoherent averaging and noise subtraction which results in an improvement in sensitivity that increases as the square root of the number of independent pulses. It is highly desirable to have an MDS of at least -25 dBZ @ 10 km to successfully observe many phenomenon of interest. Sensitivity can be increased at the expense of range resolution and/or temporal resolution.

2.1.3. Range/Velocity Ambiguity

Every radar system must compromise between unambiguous range and unambiguous velocity because unambiguous range is inversely proportional to the PRF, while unambiguous velocity is directly proportional to the PRF. Unambiguous velocity is also directly proportional to wavelength. This means that to attain reasonable unambiguous velocities, a W-band radar must operate a high PRF's. For example, to achieve a +/- 8 m/s unambiguous velocity at W-band (94 GHz), requires a PRF of 10 kHz. Operating at high PRF's also increases the likelihood of data corruption due to second trip echoes from the ground. Figure 2 illustrates this point by plotting aircraft altitude vs. radar beam incident angle for PRF's of 5 and 10 kHz. An incident angle of zero (0) represents nadir pointing. To operate at increasingly steeper incident angles, one must either reduce

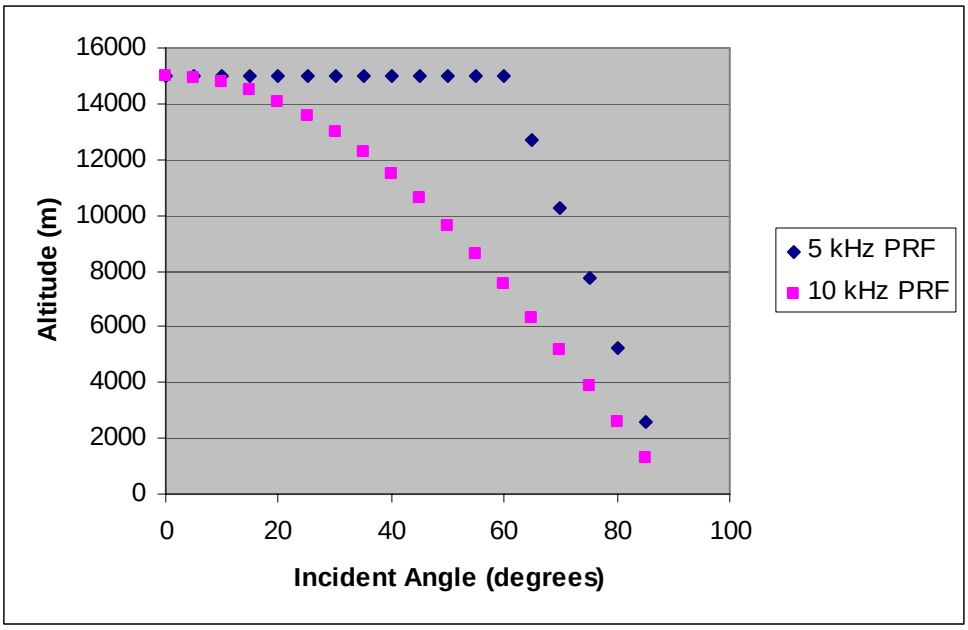

Figure 2: Maximum operating altitude as a function of incidence angle for 5 and 10 kHz.

aircraft altitude, reduce the PRF or both. Based on this illustration, it is likely that the radar will be operated at a PRF of less than 10 kHz, except when pointing nadir or above horizontal. Second trip may not be a factor for horizontal pointing (90 degree incidence) as the beam and/or sidelobes may intercept the ground at a range beyond the radar's sensitivity.

2.1.4. Velocity and Reflectivity Accuracy

As polarization capability and a second wavelength will be added in phases B and C, it is highly desirable to have reflectivity accuracies of < 1 dB to have a high degree of confidence in any differential measurements based on reflectivity e.g. ZDR or differential attenuation. Velocity accuracies of < 0.25 m/s are also highly desirable for reasonable SNR's (> 10 dB), since the atmospheric phenomenon of interest will likely have velocities on the order of a few meters/second maximum.

2.2. Upgrade Path

The phased approach of the HCR development was already mentioned in Section 1 of this document. It is essential to design and build the phase A HCR system to accommodate the upgrades introduced by phases B and C without major re-work to the radar's subsystems or to the 20" pod infrastructure. With sufficient planning during phase A, this goal should be attainable.

2.3. Size and Weight

The size and weight of the HCR is governed by the weight carrying capacity of HIAPER's center wing stores hardpoint and the physical dimensions of the 20" pod. The wing hardpoint is rated for 1000 lbs. Given an estimated pod weight of 200 lbs., there is an 800 lb. payload capacity for the HCR. The entire radar system must be contained within the volume of the 158.5" pod. The pod has a useful volume of approximately 87 cu. Ft. for radar equipment.

2.4. Operating Environment

Since the HCR will be housed in an un-pressurized, non-environmentally controlled pod, it will be subjected to the temperature, pressure, shock and vibration extremes associated with the aircraft and environment. The following environmental stresses are likely to be encountered:

Temperature	-65 C to +50 C
Pressure	1.6 psi. to 14.7 psi.
Shock	6 g, 11 millisecond duration – per RTCA/DO-160D
Vibration	8 g (rms), 10 Hz to 2000 Hz – per RTCA/DO-160D

2.5. Power and Signal

The HCR must operate using HIAPER's existing wing wiring for both power and signal. This wiring is described in detail in the G-V Investigator's Handbook

(http://www.hiaper.ucar.edu/handbook/index.html). Briefly, the following power is available to the HCR:

20 Amps, 120 VAC, 60 Hz

20 Amps, 120 VAC 60 Hz

20 Amps, 120 VAC, 400 Hz

In addition the following signal wiring is available:

8 pairs, twisted shielded twinax

50 ohm coax for IRIG-B

75 ohm coax

2, RJ-45 Gigabit Ethernet

4, Multimode fibers

3, 9 conductor shielded

2, 4 conductor shielded for ASCII

2.6. Calibration

Accurate calibration is critical to the measurement accuracy of the HCR; therefore both absolute and relative (real-time) calibrations will be implemented in the radar system design. A more detailed discussion of the calibration scheme appears in Section 3.8.

2.7. Remote/Autonomous Operation

The HCR will be designed to operate autonomously while in flight, in accordance with the design philosophy for all HIAPER Aircraft Instrumentation Solicitation (HAIS) instrumentation. To achieve this objective, the status of all mission critical sub-systems must be monitored regularly and reported via HIAPER's satcom down-link to ground observer(s). In addition, a radar control up-link will also be provided to change operational modes and/or reset the system. Self-test diagnostic capability must also be built into the design of the HCR.

3. System Design

Section 2, established the system requirements of the HCR. This section outlines a design that attempts to meet the goals of the system specification.

The HCR system design has been divided into components which include the system overview, the antenna, transceiver design, and data system design, the pod infrastructure, nose cone/radome considerations, the mechanical structure, and the system calibration. The intent is to design each system component such that the overall system meets or exceeds the previously stated requirements.

3.1. Overview

Figure 3 shows a system level diagram of the HCR. phase A system components are all shaded in aqua, while phase B and C system components are shaded in yellow and orange, respectively. The pod will house the antenna and pedestal, the receiver and transmitter (R/T) and most of the data system. In- and quadrature-phase time series data plus housekeeping will be sent via Ethernet to the cabin data system for further signal processing, display and archiving. Desired spatial coverage will be attained via a rotating reflector plate mounted at 45° to the plane of the antenna. This approach eliminates the

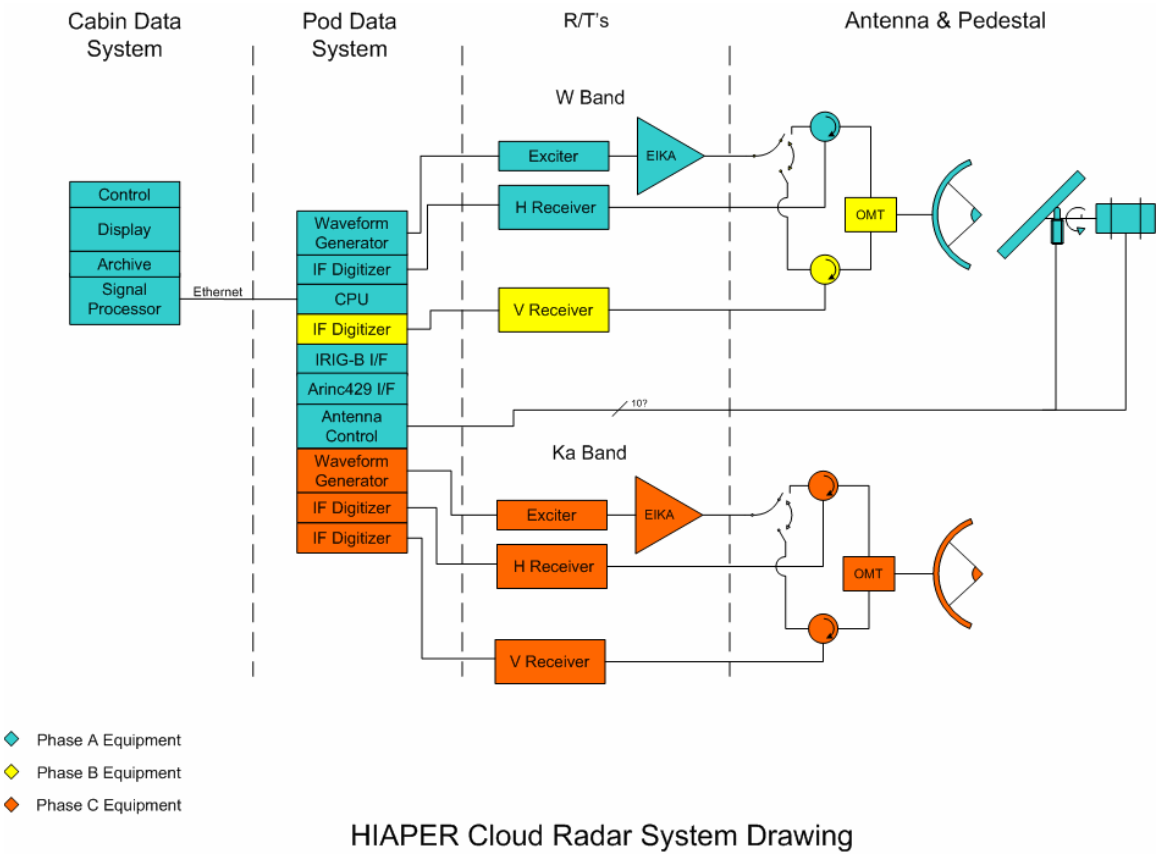

Figure 3: System level diagram of the HIAPER Cloud Radar. phase A items are colored blue, phase B item are colored yellow, and phase C items are colored orange.

loss, cost and complexity of a rotary joint. It will not only translate the radar beam from the horizontal to the vertical, but also allow the beam to be steered over at least 180° from zenith to nadir. A linear actuator which rotates with the reflector, can be used to "trim" the reflector to compensate for the pitch of the aircraft so that the effect of the horizontal component of the aircraft's velocity on the radar Doppler velocity is minimized.

3.2. Antenna

The antenna is an extremely critical part of any radar system. The antenna's effective aperture determines the radar's beamwidth and sidelobe levels. The antenna's gain and beamwidth also contribute significantly to the radar's sensitivity. The antenna can also be the limiting factor in cross-pol isolation for polarimetric systems. In this application, the pod ring-frame structure the antenna aperture to 15 inches.

The initial HCR feasibility study discussed the relative merits of two types of antennas considered suitable for the HCR: parabolic, including prime focus, Cassegrain and offset Gregorian, and lens antennas. Note, that planar arrays and their variants were not included due to their lack of fast switching polarization capability. Lens antennas at millimeter wave frequencies give superior performance in terms of peak sidelobe level and cross-pol isolation over all parabolic types with the possible exception of offset Gregorians; however, the complexity and required alignment precision of offset Gregorian antennas makes them less attractive in a pod based application where vibration and wide temperature swings exist. Although lens antennas are generally heavier and have larger f/D ratios than parabolic antennas, there is sufficient space and weight handling capability in pod to accommodate one. Estimates from Millitech place the overall antenna length at 21" and the weight at 60 lbs. Millitech also estimates antenna performance as follows:

3 dB Beamwidth	0.6 degrees
Gain	48 dBi
Peak Sidelobes	−24 dB
Cross-pol Isolation	~ 30 dB

As previously stated, a 45º rotating reflector plate in front of the antenna will be used to steer the beam to meet spatial coverage requirements. A consequence of the reflector plate is that the polarization of the transmitted waveform changes as the reflector plate rotates. This will impact phases B and C of the HCR development

Figure 4 shows the geometry of an incident electric field on a reflector plate tilted at 45 degrees to the direction of propagation of the incident electric field. The reflector plate lies in the $x''y''$ plane which is rotated by $\theta_i = 45$ degrees from the $x'y'$ plane around the y'' or y' axis. The incident electric field lies in the $x'y'$ plane and is propagating in the $\hat{z}$ direction. The electric field vector is rotated by an angle ϕ from the x' axis. The aircraft coordinate system is the xyz coordinate system.

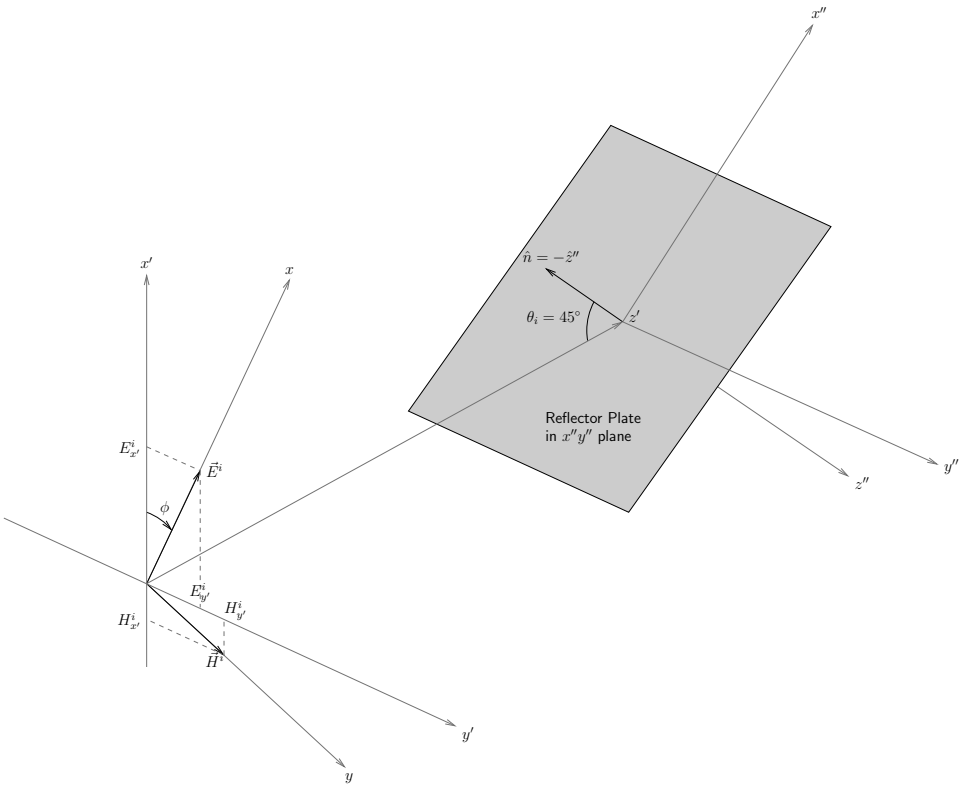

Figure 4: Incident electric field on reflector plate.

The incident electric field polarized in the $\hat{x}$ direction propagating in the $+\hat{z}$ direction is written as $\vec{E}^{\,i} = \hat{x}E_0^i e^{-jk_0 z}$. If the reflector plate is rotated counterclockwise around the z-axis by an angle ϕ, then the reflected electric field is

$$\vec{E}^{\,r} = E_0^i \left\{ -\hat{x}\sin^2\phi - \hat{y}\cos\phi\sin\phi - \hat{z}\cos\phi \right\} e^{-jk_0(x\cos\phi - y\sin\phi)}.$$

The relationship between these vectors is illustrated in Figure 5 where

$$\theta_r = \cos^{-1}\left(\cos\phi\sin^2\phi + \cos^2\phi\right).$$

The polarization of the transmitted electric field changes as the reflector plate is rotated. This will have a small effect on reflectivity measurements recorded with different scan angles, and will require a transformation to a global coordinate system for polarimetric variables. For a fully polarimetric radar (phase B of the implementation plan), since both polarizations are measured, the received signal can be rotated into any polarization basis.

3.3. Transceiver

A block diagram of the phase A transceiver (single-wavelength, single-polarization receiver) is shown in Figure 6. The transceiver consists of four main subsystems: the exciter, the receiver, the calibration network and the high power amplifier (EIKA as shown). The mechanical design of the transceiver will include space for a polarimetric switching network and the addition of the second wavelength (phases B and C). The

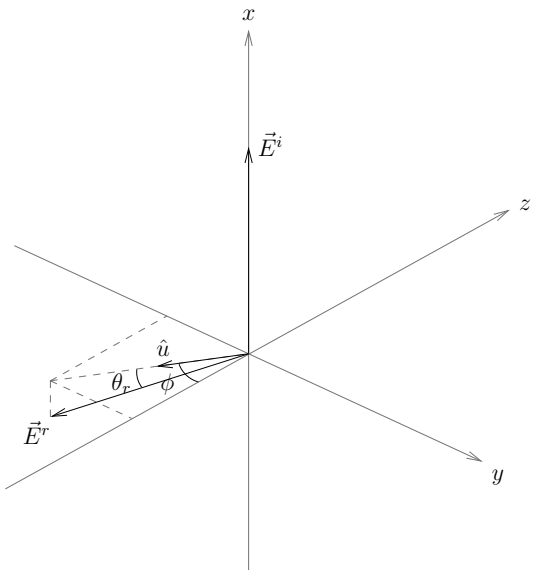

Figure 5: Incident and reflected electric field vectors for a reflector plate that is rotated by an angle φ. The incident electric field is orientated along the x axis, and the reflected electric field is rotated by an angle φ from the xz plane, and by an angle θ from the yz plane.

implementation of these extensions is not discussed in this document. The design of the transceiver subsystems is described in the following sections.

3.3.1. Exciter

The phase A system will transmit a single frequency pulse with a pulse width that ranges from 200 ns to 2 μs (30 to 300 meter range resolution) at a PRF between 1 – 20 kHz. However, to accommodate extension to a pulse compression system in phase B, the exciter will be implemented using an arbitrary waveform generator followed by a frequency up-conversion to W-band. The arbitrary waveform generator allows one to pre-distort a pulse compression waveform in amplitude and phase to compensate for amplitude and phase distortions due to microwave components in the exciter. This is necessary, as to achieve range sidelobes less than −60 dB (typical two-way sidelobe level of the antenna), the amplitude variations must be less than 0.2 % (0.03 dB) and the phase variations less than 0.115 degrees (Cook and Bernfield, 1993).

Figure 7 shows the architecture of an arbitrary waveform generator and quadrature modulator. Baseband I and Q samples are digitally up-converted to a center frequency of 125 MHz using a numerically-controlled oscillator, and then converted to analog signals using a high-speed digital to analog converter. With a DAC output rate of 500 MS/s, images of the 125 MHz signal will exist at 375 MHz. A bandpass filter with a phase linearity of ±1.5 degrees (max), and an amplitude ripple of 0.2 dB over a 20 MHz passband, is used to suppress the image by greater than 70 dB.

Figure 8 shows a frequency domain representation of the up-conversion implemented in the transceiver. The analog versions of the I and Q signals at 125 MHz up-converted to

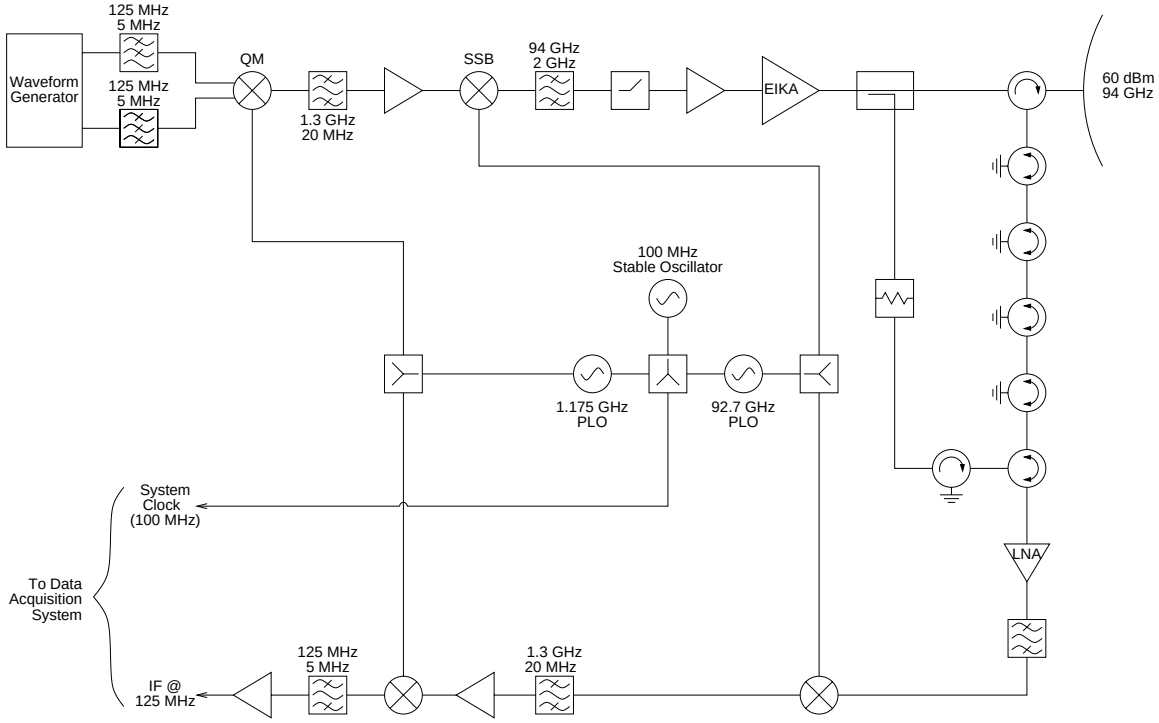

Figure 6: Block diagram of the single polarization HCR transceiver.

1.3 GHz using a quadrature modulator. Sideband suppression of greater than 20 dB can be achieved, and the lower sideband is further suppressed by a minimum of 40 dB with a bandpass filter that has a phase linearity of ±0.5 degrees (max) over a 50 MHz passband. The lower sideband will therefore be suppressed by greater than 60 dB.

The signal at 1.3 GHz is then up-converted to 94 GHz with a single-sideband modulator. The signals in the lower sideband at 91.4 and 91.65 GHz will be suppressed by a minimum of 20 and 80 dB. A bandpass filter with a center frequency of 94 GHz, and a linear phase will further suppress these signals by 26 dB as shown in Figure 8. These signals and the sideband at 93.75 GHz will be further suppressed due to the limited bandwidth of the transmitter.

3.3.2. Receiver

The phase A system will use a single channel (non-polarimetric) receiver (Figure 6). To estimate the expected performance of the receiver, typical component values have been selected from commercially available components. These values are listed in Table 1.

Figure 9 shows a frequency domain representation of the down-conversion implemented in the receiver. Received signals at W-band are filtered to suppress signals and noise in the receiver image band and then down-converted by a double sideband mixer to 1.3 GHz. Signals at the image frequency (91.4 GHz) will be suppressed by greater than 72 dB. The exact value of the images will depend in the extra suppression obtained by the transmitter, but if too large, a further 20 dB suppression can be obtained by using an image rejection mixer. The 1.3 GHz IF signal will then be filtered and down-converted to

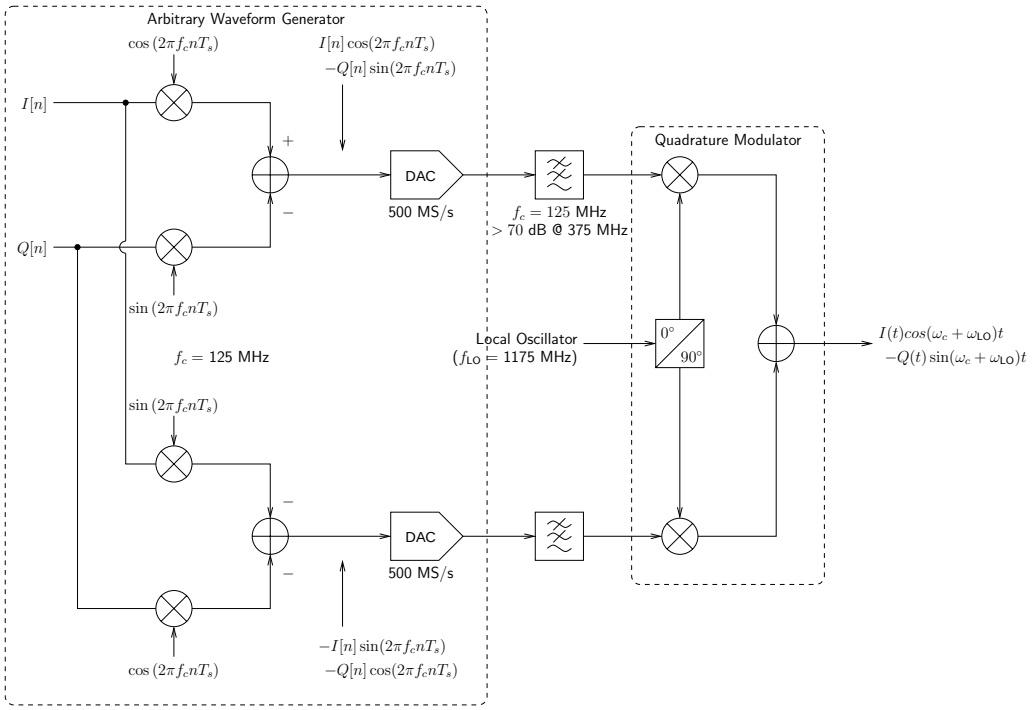

Figure 7: Waveform synthesis: baseband I and Q samples are digitally up-converted to 125 MHz. The analog output of the DACs are low-pass filtered and up-converted to 1300 MHz by a quadrature modulator.

the final IF of 125 MHz. Signals in the image band at this stage will be greater than 100 dB lower than the desired signal, and therefore a double-sideband mixer will be sufficient. This IF signal will pass through a 5 MHz bandwidth anti-aliasing filter before being sampled by the analog to digital converter.

The receiver bandwidth is determined by the minimum range resolution specification (30 meters). For a pulse width of 200 ns, the bandwidth is 5 MHz. However, the phase B system will use pulse compression to increase the average transmit power and therefore the sensitivity of the system. To achieve low range sidelobes with a pulse compression system, the spectrum of the transmitted pulse will be shaped, resulting in an increase in required receiver bandwidth for a given range resolution. To accommodate this increase in bandwidth, all of the receiver components for the phase A system, except the anti-aliasing filter before the analog to digital converter, will be specified for linear-phase 20 MHz passband to accommodate lower range resolutions. The sensitivity of the system will be optimized to the pulse length used by digitally filtering the received signal to desired signal bandwidth after digitization.

An estimate of the equivalent noise temperature of the receiver is calculated using

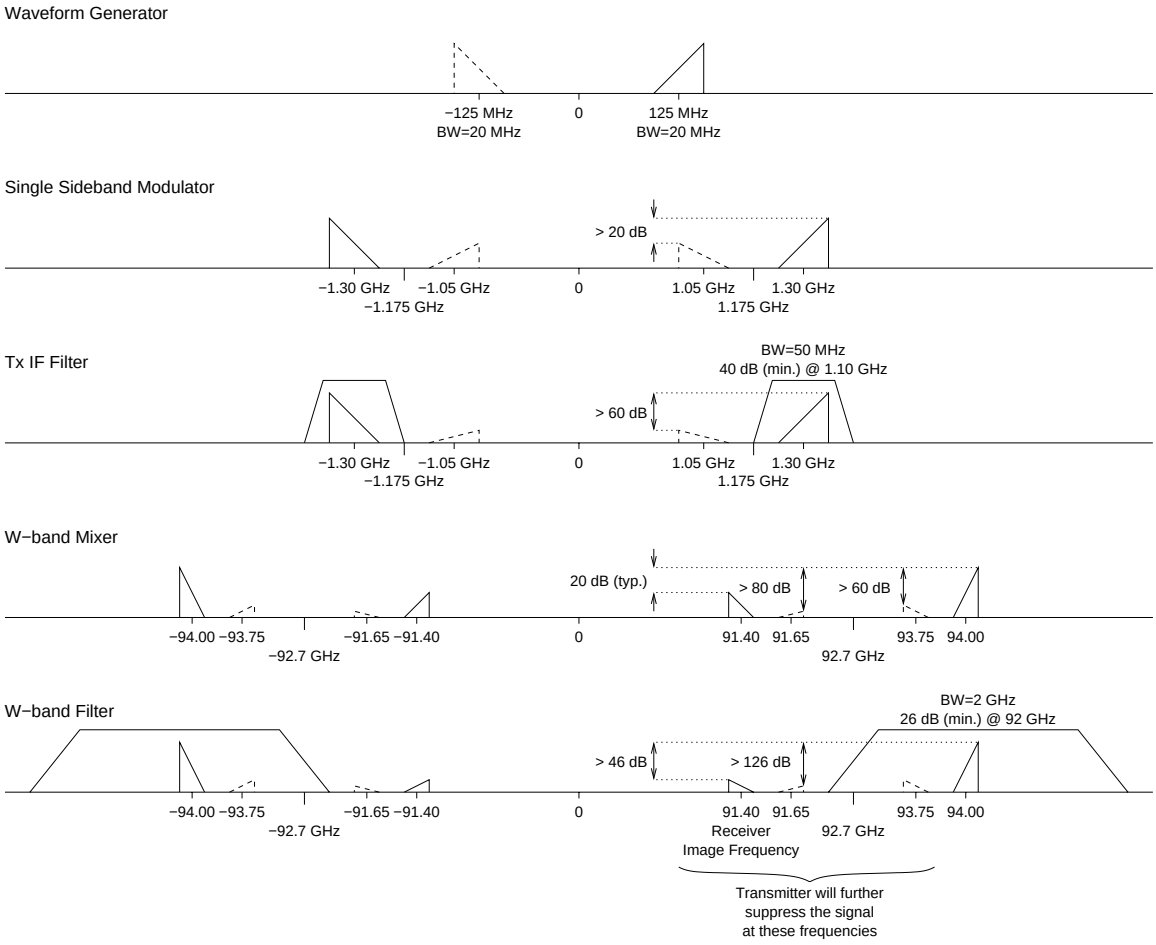

Figure 8: Two stage heterodyne frequency up-conversion.

$$\left(T_e\right)_N = \left(T_e\right)_1 + \sum_{i=2}^{N}\left\{\frac{\left(T_e\right)_i}{\prod_{j=2}^{i} G_{j-1}}\right\}$$

where $\left(T_e\right)_i$ and G_i are the noise temperature and gain of each component in the receiver. The receiver front-end electronics includes waveguide from the antenna to the receiver (assumed to be 1 foot for the purposes of this calculation), the TR circulator, five latching circulators, a low-noise amplifier, a bandpass filter, and a double sideband mixer. The loss through 1 foot of WR-10 waveguide is 0.8 dB/ft and each of the circulators in the front-end of the receiver has a maximum insertion loss of 0.5 dB. Commercially available W-band low-noise amplifiers have noise figures of around 4.5 dB. At an operating temperature of 273.15 K, the noise figure of the receiver is 9.35 dB which results in a noise power of -97.9 dBm at the input to the receiver in a 5 MHz bandwidth. This sets the lower end of the receiver dynamic range, and the minimum detectable signal by the receiver.

Table 1: Receiver Component Values

Component	Gain	Noise Figure	OIP3	P1dB at Output	Bandwidth
Waveguide	−0.80	0.76			
Fixed-bias circulator	−0.50	0.47			
Latching circulator	−0.50	0.47			
Latching circulator	−0.50	0.47			
Latching circulator	−0.50	0.47			
Latching circulator	−0.50	0.47			
Latching circulator	−0.5	0.47			
Low noise amplifier	20.00	4.50	30.00	−5.00	
Bandpass filter	−3.70	3.55			2000.00
Double-balanced mixer	−8.00	7.78	2.00	−8.00	
Bandpass filter (fc=1.3 GHz)	−1.00	0.95			50.00
Attenuator	−3.00	2.87			
Amplifier	37.00	3.50	28.00	17.00	
Double balanced mixer	−6.90	6.69		9.00	
Bandpass filter (fc=125 MHz, BW=5 MHz)	−2.20	2.10			5.00
Amplifier	20.00	3.70	46.00	26.00	
Attenuator	−20.00	19.74			

The upper limit of the receiver dynamic range is set by the maximum input signal to the receiver which is -22.4 for the components in Table 1. Therefore the receiver dynamic range is $-22.4 - (-97.9) = 75.5$ dB. ADC quantization noise floor is usually set around 10 dB below the receiver noise floor which means that a 14 bit ADC with a dynamic range of around 84 dB will be sufficient for the radar.

Phase noise requirements for the 94 GHz stable local oscillator (STALO) are determined by velocity accuracy specification. The transmitted and received signals are up- and down-converted using the same STALO. Phase noise causes the STALO to de-correlate in the time between between transmission of the pulse and reception of reflections from a feature. Oscillator phase noise at Allen variance lags that are smaller than the round trip time (i.e. large offset frequencies from the carrier) contribute more to the de-correlation of the received signal. Thus to calculate the variance in the velocity measurement due to phase noise of the STALO, the integrated phase noise (phase variance) of the oscillator is calculated by integrating a delay dependent phase noise spectrum.

Figure 10a shows the phase noise of a W-band STALO, Figure 10b shows the delay dependant function, and Figure 10c shows the delay-dependent phase noise spectrum used to calculate the integrated phase noise of the system. For this phase noise spectrum, the integrated phase noise or phase variance for a feature 10 km from the radar is 8.6 degrees, which translates to a velocity variance of 0.07 m/s. This is negligible compared to the uncertainty due to aircraft motion (tenths of a m/s), and therefore will contribute little to the velocity error.

The network of five ferrite latching circulators provides isolation between transmit and receive components. The EIK generates a 1.7 kW (+62 dBm) peak power pulse, and

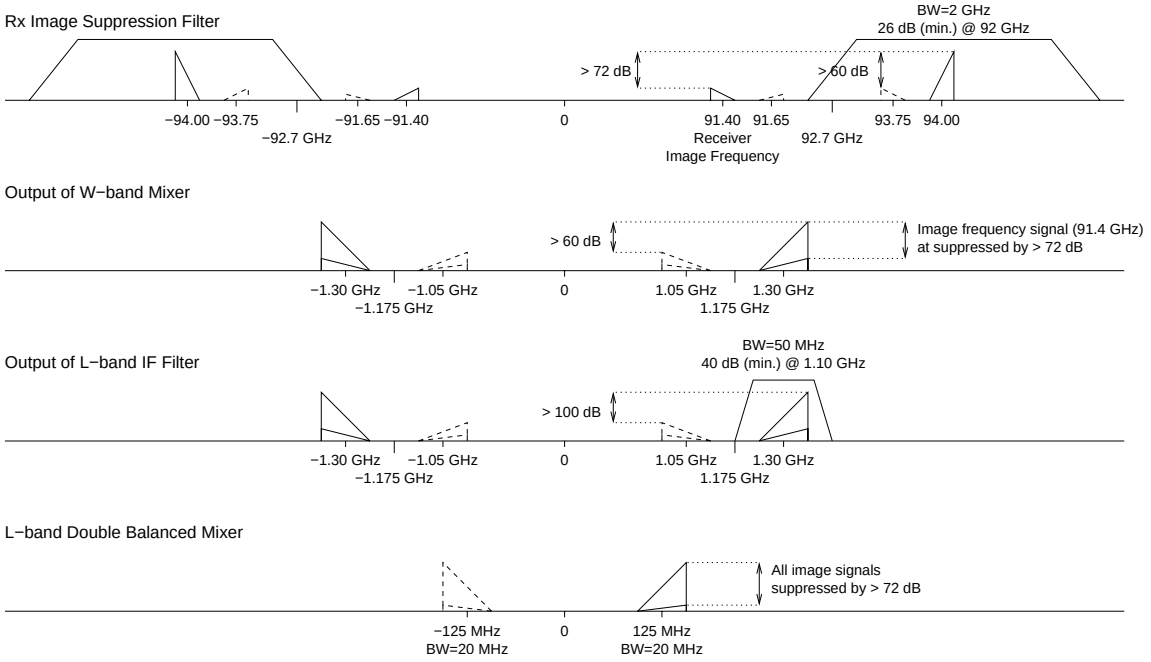

Figure 9: Down-conversion of the received signal. The first down-conversion stage converts the W-band received signal to L-band, and the second from L-band to the digital receiver intermediate frequency. Image-rejection mixers and filters are used to suppress unwanted image frequencies.

assuming that the low noise amplifiers has an absolute maximum input power of around +20 dBm, at least 42 dB of isolation is required between the output of the EIKA and the input to the low noise amplifier. Since the ferrite circulators have 25 dB of isolation (for a 1 GHz bandwidth), two circulators are sufficient to provide the necessary isolation to protect the low noise amplifier. The additional switched attenuation is required to suppress the transmit leakage pulse such that it doesn't interfere with the transmit pulse coupled through the calibration network. Insufficient isolation between the calibration signal and the transmit leakage pulse will result in amplitude and phase variations on the calibration signal.

The strongest leakage pulse will likely be reflected from the antenna due to mismatch.

Table 2: STALO Phase Noise Spectrum

Offset Frequency	**Phase Noise**
100 Hz	-40 dBc
100 Hz	-65 dBc
1 kHz	-75 dBc
10 kHz	-85 dBc
100 kHz	-95 dBc
1 MHz	-105 dBc
10 MHz	-110 dBc

Assuming an antenna return loss of 14 dB (VSWR = 1.5:1), and a transmitted peak power of +60.7 dBm at the antenna input, the leakage pulse at the input to the ferrite switches network will be 45.4 dBm (14 dB return loss, 0.8 dB waveguide loss, 0.5 dB loss through the TR circulator). The signal through the calibration path must be less than the maximum linear input signal to the LNA which in this case is around -30 dBm (5 dB below the 1 dB compression point of the LNA). Furthermore, the signal through the calibration path must dominate over the leakage signal such that amplitude and phase distortions are minimzed. The isolation required between the transmit leakage and the calibration signal is calculated by considering interference between the sum of two frequency modulated signals given by

$$v(t) = a_1 \cos(\omega t) + a_2 \cos\{\omega(t + \Delta t)\},$$

where a_1 and a_2 are the amplitudes of each waveform. Ideally, the calibration signal coupled from the transmitter would be the first term in the above expression. The second term is time-shifted version of the transmitted signal which propagates through the transmit/receive circulator. Synchronously demodulating the above signal results in

$$v_z(t) = \frac{1}{2} a_1 + \frac{1}{2} a_2 \exp(-j\omega\Delta t).$$

The amplitude and phase differences between $v(t)$ and the desired calibration signal are calculated from $|v_z(t)|$ and $arg(v_z)$. The ratio of the actual signal (calibration and transmit leakage signals) to the desired signal (calibration signal) is given by

$$\varepsilon = 1 + \frac{a_2^2}{a_1^2} + 2\frac{a_2}{a_1}\cos(\omega\Delta t).$$

The maximum and minimum values of this ratio occur when the cosine equals +1 and -1 respectively. From this, the maximum variation in the calibration signal is based only on the ratio of a_1 and a_2. To achieve an amplitude distortion of less than 0.1 dB in the calibration signal, the calibration signal must be 38.7 dB larger than the leakage signal. Therefore, at least 114.1 dB of isolation or five latching circulators is required between the calibration path and the transmitter. With five latching circulators, the ratio $\frac{a_1^2}{a_2^2}$ is 49.6 dB, and therefore the amplitude variations are 0.03 dB which is more than sufficient for the tracking calibration changes in the system.

3.3.3. High Power Amplifier

HCR will use an extended interaction klyston amplifier (EIKA) for a high power amplifier to amplify the signal for transmission. The tube to be selected for the HCR is based on the EIKA used in the CloudSat radar. The specifications of this tube are shown in Table 3.

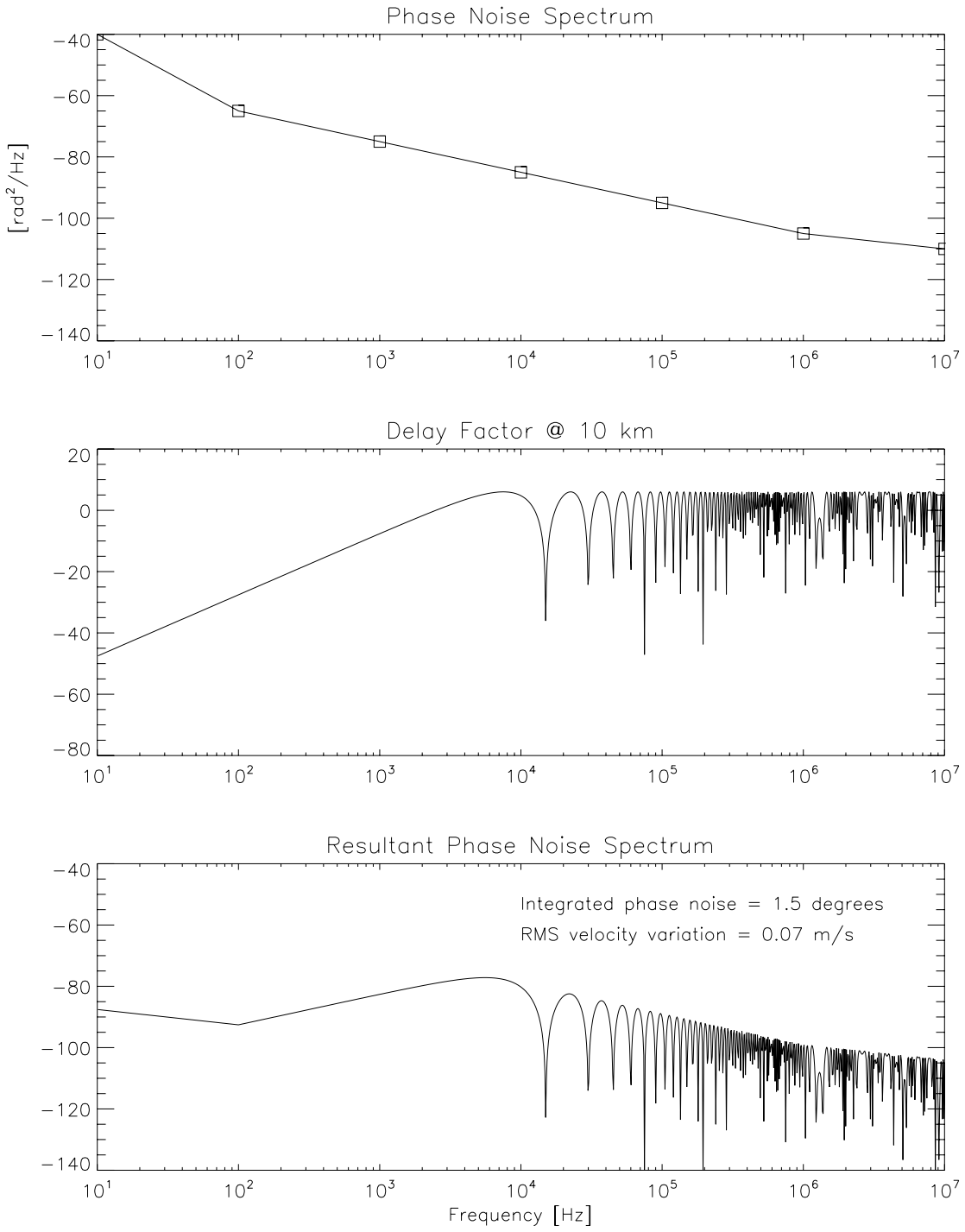

Figure 10: Specification of W-band local oscillator phase noise spectrum and resultant RMS velocity uncertainty due to local oscillator instability for features at 10 km.

The EIKA will be conduction cooled and the high voltage modulator electronics will be mounted in a pressure vessel in the pod. The modulator electronics will need to be designed to handle aircraft attitude changes and low temperature operation. The aircraft

Table 3: EIKA Specification

Parameter	W-band EIKA
Center Frequency	94.0 GHz
Bandwidth	100 MHz
Peak Power	1.7 kW
Integrated Noise	45 dBc
Gain	50 dB
Rise/Fall Time	100 - 200 ns
Amplitude Pushing Factors	
Cathode Voltage	0.0008 dB/V
Grid Voltage	0.006 dB/V
Phase Pushing Factors	
Cathode Voltage	0.14 degrees/V
Grid Voltage	0.4 degrees/V
Max. Duty Cycle	5 %
PRF Range	Single Pulse to 80 kHz (duty cycle limited)
Pulse Width Range	0.1 – 10 μs
Guarenteed Lifetime	1000 hours
Expected Lifetime	15000 hours

power supply system can cabling will need to provide around 5 Arms at a 5% duty cycle for steady state operation, and handle a peak surge of 25 A for 4 ms upon application of prime power. Ferrite switches will be located further than 2 inches away from the EIK magnets to ensure that the magnetic fields of the switches are not affected.

The waveguide will be pressurized with nitrogen to handle 1.7 kW of peak power. WR-10 waveguide can handle is 8 % of the theoretical waveguide peak power (1.38 kW at 94 GHz), assuming an antenna VSWR is 1.5:1, a pulse width of 5 μs (for pulse compression), a PRF of 10 kHz, and a side-wall directional coupler after the transmitter, and operating at an altitude of 50000 ft and a temperature of 68 F [Ciavolella, 1972].

For pulse lengths up to 1 μs and PRFs up to 10 kHz, the maximum average power is 17 W which is just less than the maximum rated average power for WR-10 (approximately 18 W at 94 GHz). The limitation on the power handling capability is predominantly due to heating in the walls of the waveguide (King 1961). The average power rating can be increased by using forced air cooling and radiating fins, and these may need to be used for long pulse lengths. However, care must be taken, since the maximum power rating decreases with increasing VSWR, due to high current points caused by standing waves, and therefore an analysis of the system will likely need to be conducted once components have been selected to determine a safe operating point.

3.4. Data System

Although the proposed radar data system is not particular to millimeter wave radars, the HCR places some unique requirements upon it; among these are size, weight and

environmental factors. For the purpose of this document, the radar data system is defined to encompass the following: radar control and timing, data display and archiving, data acquisition, signal processing and housekeeping functions. Housekeeping consists of time, antenna angle, and aircraft attitude, etc. Functionality will be divided as depicted in Figure 3.

Radar control, preliminary signal processing and data display and archiving will be performed on 19 inch rack-mount PC(s) located in the cabin, while radar timing, real-time data acquisition and housekeeping will take place in a satellite data system located in the NCAR pod. The cabin and pod data systems will be linked by the two available gigabit network connections. These connections will relay radar control commands from the cabin as well as digital timeseries data, housekeeping and status from the pod. It is intended that radar control and status information be available to ground personnel via HIAPER's sitcom link. Data rates for the phase A system are estimated at 128 Mbits/sec which should be easily handled by a single gigabit Ethernet connection. Phase B and C data rates are estimated at 340 Mbits/sec and 680 Mbits/sec, respectively. It is likely phase C would require the use of both network connections for data.

3.4.1. Pod Data System

The basic functional components of the pod data system are shown in Figure 3. Due to the rugged environment of the pod and the limited space available, the data system will consist of compact PCI cards mounted in an Air Transport Rack (ATR) form factor. Commercial compact PCI (cPCI) offerings support the required data system functionality, while the ATR can provide solutions to the vibration and temperature extremes to be encountered.

A single board computer (SBC) running Linux will handle local supervisory tasks and communications (data, status and control) with the in-cabin host data system. This card is represented by the CPU block in the diagram. The OS and operational software will be stored on a solid state drive located onboard the SBC. The remainder of the pod data system will provide data acquisition, radar timing, transmit waveform generation antenna control (reflector plate positioning) and housekeeping functionality. Aircraft attitude will be obtained from the aircraft's IRU via ARINC-429 provided by a twinax connection. Time will be obtained from the aircraft's IRIG-B time code via the 50 ohm coax cable. It is possible that network time protocol (NTP) can be used to time tag data rather than IRIG-B and this option will be explored before the critical design review (CDR). Position and control (both rotational and linear) of the reflector plate can be accomplished via commercial two-axis motion control hardware using quadrature feedback from an optical encoder as well as feedback from a couple of two-axis inclinometers, one in pod and the other in cabin. The inclinometers will measure the differential pitch and roll changes between the pod and the fuselage. This information along with pitch and roll from the aircraft's inertial reference unit (IRU) can be used to re-position the reflector plate in-flight and can also be recorded for post-flight correction of pointing and velocity.

Radar timing, IF digitization and transmit waveform generation will be performed in commercial FPGA based software defined radio (SDR) circuit boards. Whether this functionality can be implemented in a single board depends on the particular vendor selected. The relatively wide-band receiver required for pulse compression in phase B

will also impact the choice of vendor.

Due to the limited antenna aperture and low peak transmit powers realistically attainable within the confines of the NCAR pod, pulse compression techniques will be employed in phase B to attain the required sensitivity. Pulse compression entails transmitting a coded pulse whose bandwidth equals that for the range resolution desired, but whose length is significantly longer than the desired range resolution. In this way, more average power can be transmitted, which increases sensitivity. The radar return is decoded and the desired range resolution is obtained. Some disadvantages of pulse compression include increased minimum range due to the longer transmit pulse and smearing of strong signals into adjacent range bins (range-time sidelobes). Pulse compression also introduces complexity into the areas of data acquisition and signal processing. The additional complexity required to both encode the transmit IF signal and decode the IF return signal can be completely handled by the profusion of COTS hardware developed for military SDR applications. This technology implements reconfigurable hardware which has the flexibility to code and decode IF signals in real-time. Current SDR developments are being undertaken to upgrade the signal processors for NCAR/EOL wind profilers and the ELDORA airborne Doppler radar, and we plan to use the expertise gained from these developments in the HCR development.

3.4.2. In-Cabin Data System

Radar product generation, data display and archiving are performed by the in-cabin data system which consists of one or more high performance rack-mount PC's. Time series data will be processed to yield spectral moments and their derivatives. Later in phases B and C, polarimetric quantities will also be computed. These parameters are displayed locally on a rack-mount LCD flat panel monitor and can be made available to other users via HIAPER'S internal data network, if desired. Calculations based on a single precision 1024 point complex FFT benchmark for a 3.6 GHz Pentium 4 chip running an fftw3 in-place algorithm (http://www.fftw.org/speed/Pentium4-3.60GHz-icc/) for 500 range gates at a 20% efficiency yield a computation time of 19.7 milliseconds. This seems to indicate that there is sufficient computational power in a single CPU to compute a power spectrum for each range gate as well as its spectral moments. Data display and archiving may require an additional PC. A preliminary data rate analysis shows that the phase A HCR will generate ~60 gigabytes/hr of timeseries data. Today's conventional storage technology lacks sufficient capacity store the raw timeseries data; however, limited quantities of raw timeseries data will be recorded to redundant removable hard drives. It is envisioned that researchers can select a range of gates as well as a time period over which to record timeseries data. Timeseries recording can also be automated, whereby a threshold based on SNR could be used to determine whether the timeseries for a given range gate is recorded. In either case, timeseries recording will be disabled once allocated disk space has been exhausted. In addition, zeroeth, first, and second moment data will also be recorded for all range gates.

3.5. System Control

It is envisioned that operational control of the HCR can be performed from within a GUI residing on one of the in-cabin data system PC's or eventually, from a PC on the ground.

In either case, control commands would be sent from the in-cabin PC to the pod SBC for execution via Ethernet. For the case of remote operation from the ground, HIAPER's sitcom up-link would be used.

3.6. Pod Infrastructure

Pod infrastructure refers to the electro-mechanical structure required to house and mount the various radar subsystems within the pod. This includes, but is not limited to, a pressure vessel to house high-voltage portions of the transmitter, the reflector plate and its associated positioning equipment, and structure to mount the receiver(s), antenna, data system, EIKA and pressure vessel.

At this stage, it is envisioned that the pressure vessel will house the EIKA and its associated modulator and high voltage power supply, as well as the IF portion of the receiver and the entire exciter (see Figure 11). The mechanical design and fabrication will be done by Design and Fabrication Services (DFS) at NCAR/EOL. They will also generate the necessary drawings and documentation for FAA certification of the structure. At this point, most of the mechanical design work must wait until after the CDR when specific radar components have been selected. Of course some iteration must

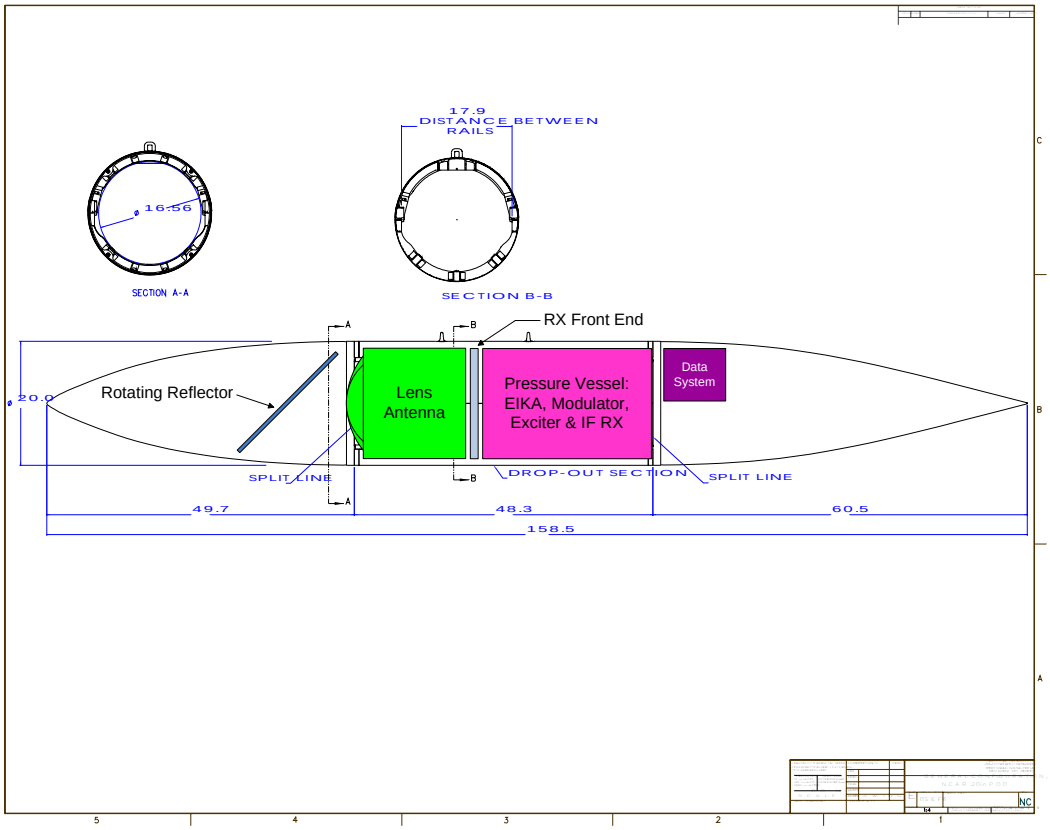

Figure 11: HCR Equipment Layout.

occur with DFS so that components which are unduly large or heavy will not be selected.

The reflector plate will be constructed of aircraft grade aluminum, machined to a flatness of 0.005" rms. Precise positioning of the plate relative to the antenna is required to avoid beam distortion, and spillover. A direct-drive DC stepper motor coupled with an optical shaft encoder will be used to positioning the plate precisely. A brushless DC motor would also be a good choice if it is determined that more torque and acceleration are required.

3.7. Nose Cone/Radome

Part of the pod's nose cone must also function as a radome for the HCR. Design of low loss airborne millimeter wave radomes is a highly specialized field. This problem is complicated by the fact that the HCR requires the radome to be highly transmissive at both the K_a-and W-bands. Several radome manufacturers were contacted regarding building a suitable radome for the HCR. Two replied favorably and provided tentative performance specifications. One-way loss through the radome is projected to be ~0.5 dB for W-band and ~0.2 dB for K_a-band. The radome will also distort the relative phases of the incident wavefront due to its curvature. The impact on the far-field beam pattern will be determined by ray tracing the reflector plate/radome structure. If phase compensation is required, it can be accomplished by adding low-loss dielectric SAN foam to the reflector plate and varying its thickness appropriately.

3.8. Calibration

Obtaining an accurate system calibration is essential if the HCR is going to fulfill its scientific mission. Both an absolute calibration, which includes reflection measurements from a target of known radar cross-section, and an internal calibration, which tracks changes in receiver gain with temperature, are required.

For a polarimetric radar system, internal calibration is important to track changes in the receiver gains. Common schemes include well calibrated test signal, noise source, or injecting a small part of the transmitted signal into both receivers. All schemes are feasible, but using the transmitted signal to track differential changes in the receiver gains also allows one to monitor the transmitted pulse. This is important when using frequency modulation since one can then compensate for phase nonlinearities due to the transmitter in the compression filter.

In this calibration scheme, it is important to achieve high isolation between the transmitter and the receiver. Coherent leakage can cause fluctuations in the calibration signal. To achieve fluctuations less of ±0.05 dB, the unwanted leakage of the transmitted pulse through other parts of the circuit must be 45 dB below the calibration signal.

In addition to monitoring differential changes in the receiver gain, we propose to monitor the transmitted pulse power during operation. This will allow us to calibrate to the system as it is likely that the transmitted power will change with temperature system change during flight.

Absolute calibration will require the use of a trihedral corner reflector positioned in a clutter and multipath free environment. It is likely to be a ground-based measurement, but could also be done in the air if the corner reflector was positioned high enough above the

ground such that ground contamination in range sidelobes could be negligible. Propagation affects such as attenuation will need to be known to obtain a good calibration. This may require in-situ measurements.

Ocean surface measurements have also been used to calibrate W-band airborne and spaceborne radars (Durden et al. 1994). This technique has been proposed as a calibration reference for Cloudsat (Stephens et al. 2002). Measurements of the ocean surface at 94 GHz have shown good agreement with quasi-specular ocean surface scattering models for low incidence angles (Li et al. 2003). However, these measurements have shown that attenuation due to water vapor and oxygen absorption affect calibration targets such as the ocean surface and thus vertical in situ profiles are required to fully calibrate the radar. Furthermore, the normalized radar cross section of the ocean surface at these incidence angles is dependent on wind speed, thus requiring in situ measurements of near surface winds by dropsondes (Li et al. 2004).

4. Estimated Performance

Performance for the phase A version of the HCR has been estimated based on our discussions with various vendors of millimeter wave components and our assessment of the state of the art of these components. Key characteristics of the HCR are summarized in

Table 4: HCR Characteristics

Parameter	
Frequency	94.0 GHz
Polarization	H
Peak Transmit Power	1.5 kW
Receiver Noise Figure	9.4 dB
Antenna Diameter	0.38 m
Antenna Gain	48 dBi
3 dB Beamwidth	0.6°
PRF	1-20 kHz
Range Resolution	30 – 300 m

Section 2.1 discussed performance goals for the HCR in terms of reflectivity and velocity accuracies, minimum detectable signal (MDS) and range/velocity ambiguity. For analysis, the PRF is 10 kHz, the dwell time is 120 ms, and the pulse width is 0.25 μs. Given this mode of operation, we can expect the following radar performance:

Table 5: System Performance

Parameter	
Range Resolution	37.5 m
Unambiguous Range	15 km
Unambiguous Velocity	+/− 8 m/s
Along Track Resolution @ 5 km	50 m
Reflectivity Accuracy (W=0.5 m/s)	0.4 dB
Velocity Accuracy (SNR=10dB, W=2 m/s)	0.2 m/s
MDS	See figure

MDS was also calculated using two very different atmospheric conditions; the first case assumes a uniform water vapor concentration of 2.5 g/cm3, while the second assumes uniform rain falling at a rate of 10mm/hr. Figure 12 shows the W-band MDS for both scenarios. It can be seen that for moderate rain, the HCR MDS increases rapidly. This is due to the severe attenuation (5 db/km one-way) of electromagnetic waves at W-band in these conditions. Under more “normal” atmospheric conditions, the MDS is estimated to be −18 dBZ at a 10 km range. Note, that this is significantly less than our desired goal of −25 dBZ. The phase B system addresses this weakness through the use of pulse compression to increase radar sensitivity by 6+ dB. It is also possible to increase the sensitivity of the phase A system by decreasing the range resolution (increasing the pulsewidth) and/or increasing the dwell time.

Figure 12: Minimum detectable signal versus range.

5. Operational Readiness

The HCR is a complex radar requiring a coordinated multi-disciplinary engineering effort and, as such, gauging the exact date when the radar will be operational on HIAPER is difficult. The goal is to deliver the radar system by June of 2008.

6. References

Ciavolella, J., 1972: Take the hassle out of high power design. *Microwaves*, June Issue.

Cook, C. E. and M. Bernfield, 1993: Radar Signals: An Introduction to Theory and Application., Artech House, Inc.

Durden, S. L., E. Im, F. K. Li, W. Ricketts, A. Tanner, and W. Wilson, 1994: ARMAR: An airborne rain-mapping radar. *J. Atmos. Oceanic Technol.*, 11, 727-737.

King, H. E., 1961: Rectangualr waveguide theoretical CW average power rating. *IRE Trans. On Microwave Theory and Techniques*, 9, 349-357.

Li, L., G. M. Heylmsfield, P. E. Racette, and L. Tian, 2003: Calibration of a 94 GHz airborne cloud radar using measurements from the ocean surface. Preprints, 31st Conf. on Radar Meteorology, Seattle, WA, Amer. Meteor. Soc., 204-206.

Stephens, G. L., and Coauthors, 2002: The CloudSat mission and the A-train. *Bull. Amer. Meteor. Soc.*, 83, 1771-1789.